water

MDPI

Article

Partitioning of Heavy Rainfall in the Taihang Mountains and Its Response to Atmospheric Circulation Factors

Qianyu Tang [1,*], Zhiyuan Fu [1], Yike Ma [1], Mengran Hu [2], Wei Zhang [3], Jiaxin Xu [1] and Yuanhang Li [1]

[1] School of Resources Environment and Tourism, Anyang Normal University, Anyang 455000, China; 13313994380@163.com (Z.F.); 13938683672@163.com (Y.M.); xjxpasl163@163.com (J.X.); 13283986597@163.com (Y.L.)
[2] Anyang National Climate Observatory, Anyang Meteorological Bureau, Anyang 455000, China; huxiao612@163.com
[3] College of Geographical Sciences, Liaoning Normal University, Dalian 116029, China; zhangweilnu@163.com
* Correspondence: tangqianyu6@126.com

Abstract: The spatial and temporal distribution of heavy rainfall across the Taihang Mountains exhibits significant variation. Due to the region's unstable geological conditions, frequent heavy rainfall events can lead to secondary disasters such as landslides, debris flows, and floods, thus intensifying both the frequency and severity of extreme events. Understanding the spatiotemporal evolution of heavy rainfall and its response to atmospheric circulation patterns is crucial for effective disaster prevention and mitigation. This study utilized daily precipitation data from 13 meteorological stations in the Taihang Mountains spanning from 1973 to 2022, employing Rotated Empirical Orthogonal Function (REOF), the Mann–Kendall Trend Test, and Continuous Wavelet Transform (CWT) to examine the spatiotemporal characteristics of heavy rainfall and its relationship with large-scale atmospheric circulation patterns. The results reveal that: (1) Heavy rainfall in the Taihang Mountains can be categorized into six distinct regions, each demonstrating significant spatial heterogeneity. Region I, situated in the transition zone between the plains and mountains, experiences increased rainfall due to orographic lifting, while Region IV, located in the southeast, receives the highest rainfall, driven primarily by monsoon lifting. Conversely, Regions III and VI receive comparatively less precipitation, with Region VI, located in the northern hilly area, experiencing the lowest rainfall. (2) Over the past 50 years, all regions have experienced an upward trend in heavy rainfall, with Region II showing a notable increase at a rate of 14.4 mm per decade, a trend closely linked to the intensification of the hydrological cycle driven by global warming. (3) The CWT results reveal significant 2–3-year periodic fluctuations in rainfall across all regions, aligning with the quasi-biennial oscillation (QBO) characteristic of the East Asian summer monsoon, offering valuable insights for future climate predictions. (4) Correlation and wavelet coherence analyses indicate that rainfall in Regions II, III, and IV is positively correlated with the Southern Oscillation Index (SOI) and the Pacific Warm Pool (PWP), while showing a negative correlation with the Pacific Decadal Oscillation (PDO). Rainfall in Region I is negatively correlated with the Indian Ocean Dipole (IOD). These climatic factors exhibit a lag effect on rainfall patterns. Incorporating these climatic factors into future rainfall prediction models is expected to enhance forecast accuracy. This study integrates REOF analysis with large-scale circulation patterns to uncover the complex spatiotemporal relationships between heavy rainfall and climatic drivers, offering new insights into improving heavy rainfall event forecasting in the Taihang Mountains. The complex topography of the Taihang Mountains, combined with unstable geological conditions, leads to uneven spatial distribution of heavy rainfall, which can easily trigger secondary disasters such as landslides, debris flows, and floods. This, in turn, further increases the frequency and severity of extreme events.

Keywords: Taihang Mountains; spatiotemporal distribution; atmospheric circulation factors; wavelet transform

Citation: Tang, Q.; Fu, Z.; Ma, Y.; Hu, M.; Zhang, W.; Xu, J.; Li, Y. Partitioning of Heavy Rainfall in the Taihang Mountains and Its Response to Atmospheric Circulation Factors. *Water* **2024**, *16*, 3134. https://doi.org/10.3390/w16213134

Academic Editor: Francesco De Paola

Received: 23 September 2024
Revised: 25 October 2024
Accepted: 28 October 2024
Published: 1 November 2024

1. Introduction

Heavy rainfall ranks among the most severe and frequent meteorological disasters [1]. It can directly cause flash floods and trigger secondary events such as landslides and debris flows. Flash floods often lead to rising river levels, damage to hydraulic infrastructure, flooding of agricultural land, disruptions to telecommunications, and even loss of life [2]. In recent years, driven by China's rapid economic growth, the damage from natural meteorological disasters has significantly increased. In the 1990s, the average annual direct economic loss due to heavy rainfall was approximately 186.7 billion RMB, but by the early 21st century, this figure had risen to over 400 billion RMB per year [3]. Consequently, studying heavy rainfall is critical for protecting lives and property.

Studying heavy rainfall in the Taihang Mountains is particularly important. As a natural boundary between China's second and third topographic steps, the Taihang Mountains feature complex topography with notable elevation differences between plains, mountains, and plateaus. These geographical characteristics significantly influence air movement, resulting in uneven spatial distribution of heavy rainfall. Additionally, the region's unstable geological conditions make it particularly susceptible to secondary disasters such as landslides, debris flows, and floods, exacerbating the frequency and severity of extreme events in areas regularly affected by heavy rainfall. Furthermore, the dense population and rapid socioeconomic development in the Taihang Mountains have led to economic losses amounting to billions of RMB in recent years due to heavy rainfall [4,5], significantly affecting societal development and livelihoods [6,7]. Over recent years, several scholars have employed numerical simulations to study heavy rainfall events in this region. For instance, Hou Ruiqin et al. [8] used the MM5 model to simulate the heavy rainfall event in south-central Hebei on 5 July 2007, discussing the influence of the Taihang Mountains on rainfall patterns in Hebei. Yan Guanhua et al. [9] conducted sensitivity experiments on the Taihang Mountains' terrain, simulating how changes in mountain height affected three typical heavy rainfall events in North China. Their results concluded that the terrain differently impacts various types of rainfall processes. Lin Huimin et al. [10] analyzed the extraordinary rainfall event in North China on 19 July 2016, using numerical simulations and concluded that both circulation and terrain had a significant influence on the event. They noted that increased terrain height enhances the blocking and uplifting of air currents, thereby intensifying precipitation. Despite these advances, only a few researchers have employed the Mann–Kendall mutation test, wavelet analysis, and Empirical Orthogonal Function (EOF) method to study the spatiotemporal evolution of heavy rainfall in the Taihang Mountains [11–13]. While EOF effectively illustrates the structural variations in climate variable fields across large regions, it struggles to accurately capture the characteristic distributions of different geographic areas and is susceptible to sampling errors [14]. In contrast, the Rotated Empirical Orthogonal Function (REOF) method offers a more precise representation of characteristic distributions across different geographic regions. REOF simplifies the spatial structure, clearly depicts regional changes, reveals correlations between regions, and reduces sampling errors [15]. The complexity of the Taihang Mountains' topography and circulation underscores the necessity of employing the REOF method for regional partitioning studies of heavy rainfall. This study aims to achieve the following objectives: (1) To apply the REOF method to investigate the spatiotemporal variation of heavy rainfall in the region. (2) To use Continuous Wavelet Transform (CWT) to explore the periodic characteristics of heavy rainfall in each subregion. (3) To apply Pearson correlation analysis, Cross Wavelet Transform (XWT), and Wavelet Coherence Transform (WTC) to examine the response of heavy rainfall subregions to atmospheric circulation factors, ultimately providing a scientific basis for disaster prevention and mitigation efforts in the region. Combining REOF-based partitioning with Continuous Wavelet Transform enables a more detailed study of the periodic characteristics of heavy rainfall in each region, facilitating the development of more targeted disaster prevention and mitigation strategies. In regions with pronounced rainfall periodicity, drainage systems and emergency supplies can be pre-deployed to mitigate secondary disasters caused by heavy rainfall. Utilizing

REOF-based partitioning of heavy rainfall, Pearson correlation analysis, Cross Wavelet Transform (XWT), and Wavelet Coherence Transform (WTC) were applied to analyze the response of each subregion to atmospheric circulation factors. Future research should incorporate circulation factors into heavy rainfall forecasting models to improve forecast accuracy, thereby offering stronger scientific support for disaster prevention and mitigation efforts in the Taihang Mountains.

2. Materials and Methods

2.1. Study Area

The Taihang Mountains (34°34′–40°43′ N; 110°14′–116°34′ E) have an elevation range of 6 to 3074 m, with the highest peak situated in Wutai County, Shanxi Province. Acting as the natural boundary between China's second and third topographic steps, the mountains are flanked by the North China Plain to the east and the Loess Plateau to the west. The region encompasses diverse and complex terrain, including plains, mountains, hills, basins, and plateaus (Figure 1). The area is characterized by well-developed river systems, with numerous rivers (Figure 1) belonging to either the Haihe or Yellow River systems [16]. Notable rivers such as the Yongding, Juma, Tang, Dasha, Hutuo, Mian, Qingzhang, Zhuozhang, Anyang, and Qi Rivers are part of the Haihe River system, while the Dan and Qin Rivers belong to the Yellow River system.

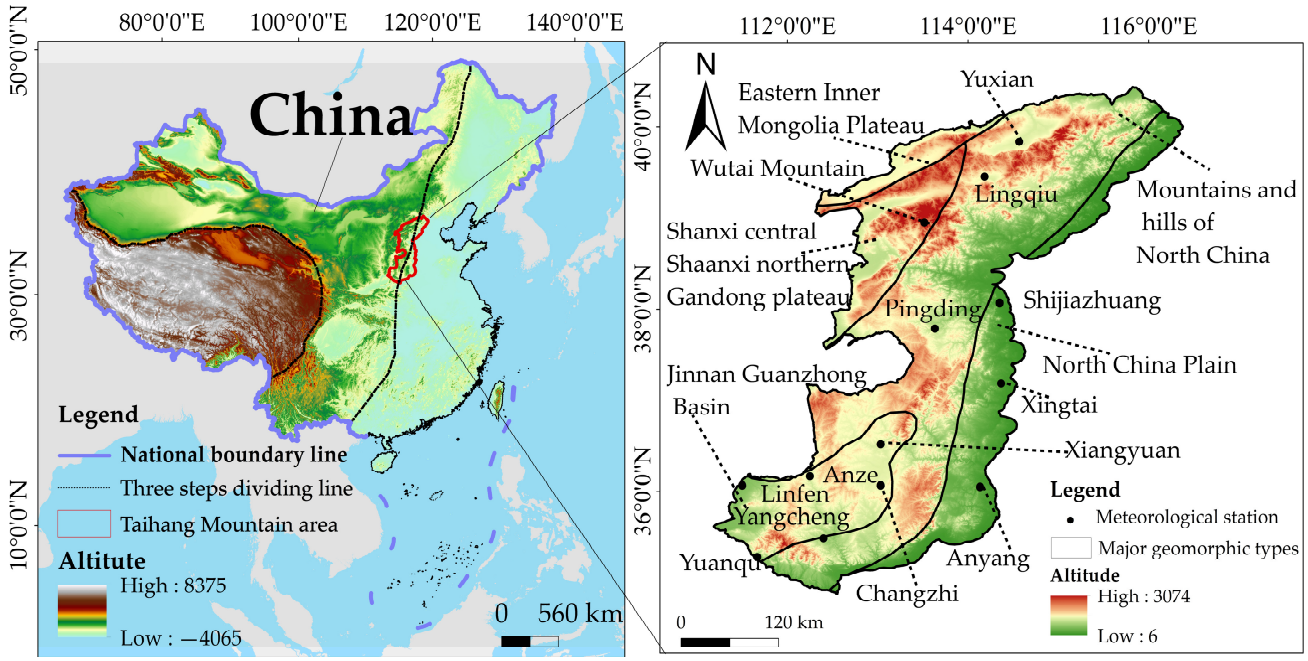

Figure 1. Schematic diagram of the study area.

The region experiences a temperate continental monsoon climate with distinct seasonal variations. The multi-year average temperature is approximately 10 °C, while the average annual precipitation is 570 mm [17]. Precipitation is mainly concentrated in July and August, accounting for 60% to 70% of the annual total. These months also record the highest frequency of heavy rainfall events, constituting roughly 77.4% of the yearly heavy rainfall occurrences. The unique geographical location of the Taihang Mountains significantly impacts the local climate. The eastern side functions as a transition zone between the North China Plain and the mountains, where the summer southeast monsoon is uplifted by the terrain, causing orographic rainfall and resulting in higher precipitation. In contrast, the western region, located on the leeward side of the southeast monsoon, receives comparatively less rainfall [18]. The unique geographical features of the Taihang Mountains greatly shape the local climate. The eastern flank, acting as a transition from the

North China Plain to the mountains, facilitates the uplift of the summer southeast monsoon, resulting in orographic rainfall and increased precipitation. Conversely, the western side, positioned on the leeward side of the southeast monsoon, experiences significantly less rainfall [18].

2.2. Data

The precipitation data for this study were sourced from the daily dataset of the Surface Meteorological Data Database, accessible through the China Meteorological Data Sharing Service Network (http://data.cma.cn, accessed on July 2023). In accordance with the classification standards for rainstorm disasters [19], rainfall events with a 24 h precipitation of $\geq$50 mm are classified as "rainstorms". A statistical analysis was performed on rainstorm events recorded at 13 meteorological stations in the Taihang Mountains region, all of which have complete meteorological records from 1973 to 2022 (Figure 1 shows the station locations, and Table 1 presents the station information). The circulation indices utilized in this study include the North Atlantic Oscillation Index (NAO), Pacific Decadal Oscillation Index (PDO), Arctic Oscillation Index (AO), Southern Oscillation Index (SOI), Western Pacific Index (WP), North Pacific Index (NP), Indian Ocean Dipole Index (IOD), and Pacific Warm Pool Index (PWR). These data were obtained from the Earth System Research Laboratory (https://psl.noaa.gov/data/climateindices/list/, accessed on July 2023), with complete records of the selected circulation indices for the period from 1973 to 2022, ensuring no missing values.

Table 1. Meteorological station data for the Taihang Mountains region.

Station ID	Station Name	Lat/N	Lon/E	Elevation/m
53588	Wutai Mountain	38.95	113.52	1302.12
53593	Yu County	39.83	114.57	1407.95
53594	Lingqiu	39.45	114.18	1363.51
53687	Pingding	37.78	113.63	1176.18
53698	Shijiazhuang	38.07	114.35	1213.22
53798	Xingtai	37.18	114.37	1115.86
53868	Linfen	36.07	111.5	971.92
53877	Anze	36.17	112.25	988.86
53882	Changzhi	36.07	113.03	980.39
53884	Xiangyuan	36.52	113.03	1029.07
53898	Anyang	36.05	114.13	987.8
53968	Yuanqu	35.28	111.67	884.08

2.3. Analysis Methods

2.3.1. Rotated Empirical Orthogonal Function (REOF)

REOF builds upon EOF decomposition by selecting eigenvectors that meet the cumulative variance contribution threshold and using them as new loading eigenvectors. These eigenvectors are then subjected to maximum variance rotation, which concentrates the high loading eigenvectors into fewer variables. This process maps the information features of the original climate vector field onto the spatial dimensions represented by the loading field. Notably, REOF applies maximum orthogonal variance rotation to the principal components, significantly enhancing the spatial partitioning capability of the climate vector field. This is especially relevant in regions with complex terrain, such as the Taihang Mountains, where it substantially improves the accuracy of rainfall spatial distribution. Given the considerable terrain variations in the Taihang Mountains, where the uplift and barrier effects of the topography significantly influence the spatiotemporal distribution of rainfall, REOF effectively captures the heterogeneity in rainfall caused by these local features. This provides a more detailed representation of the spatial structure of the climate field [20,21]. This method reduces noise in the decomposition of climate fields and improves the understanding of regional climate variability. It allows for a more detailed depiction of spatiotemporal rainfall characteristics across different geographical

regions [22]. For detailed calculation methods and the theoretical foundations of REOF, refer to [23].

2.3.2. Mann–Kendall Trend Test

The Mann–Kendall trend test is a non-parametric statistical method commonly used to detect trend changes in time series data [24]. This method is based on rank comparisons and does not require specific distribution assumptions, making it suitable for non-normally distributed data [25]. The M–K trend test determines whether a significant trend exists in the data series by calculating the test statistic S and variance $Var(s)$, followed by a significance test using the standardized test statistic Z.

For a given time series, $X_t(t = 1, 2, 3 \ldots, n)$, the calculation formula for the test statistic S is:

$$S = \sum_{k=1}^{n-1} \sum_{j=k+1}^{n} \mathrm{sgn}(X_j - X_k) \tag{1}$$

where X_j and X_k are the corresponding years of the heavy rainfall time series, and sgn is the sign function. The formula for the variance $Var(S)$ calculation is:

$$Var(S) = \frac{n(n-1)(2n+5)}{18} \tag{2}$$

where $Var(S)$ represents the variance of the test statistic, and n denotes the sample size of the heavy rainfall time series. To assess the significance of the test statistic S, the standardized test statistic Z is further calculated, with the formula given as:

$$Z = \begin{cases} \frac{S-1}{\sqrt{Var(S)}}, S > 0 \\ 0 \quad , S = 0 \\ \frac{S+1}{\sqrt{Var(S)}}, S < 0 \end{cases} \tag{3}$$

When the test statistic Z is less than 0, it indicates a decreasing trend in heavy rainfall; when the MK test statistic Z is greater than 0, it indicates an increasing trend. Furthermore, if the absolute value of the test statistic Z exceeds 1.96, the trend is considered significant ($p < 0.05$) [26].

2.3.3. Wavelet Analysis

Wavelet analysis can analyze instantaneous and time-varying signals in a time series while simultaneously localizing signals in both the time and frequency domains, enabling the extraction of useful information from the signals. Using dilation and translation, wavelet analysis allows for multi-scale analysis of functions or frequency signals [27]. This study employs the Continuous Wavelet Transform (CWT), which is used to analyze the characteristics of signals at different scales and temporal positions. For the original time series $X(t)$, its Continuous Wavelet Transform is defined as:

$$W_X(T, S) = \int_{+\infty}^{-\infty} x(t) \cdot \psi^*_{T,S}(t) dt \tag{4}$$

In Equation (1), $\psi(t)$ represents the wavelet function, and $\psi^*_{T,S}(t)$ is the complex conjugate of the wavelet function. The Continuous Wavelet Transform reflects the variance of the original time series within a certain time–frequency range, where larger fluctuations indicate greater variability in the time series [28].

Cross Wavelet Transform (XWT) is used to analyze the frequency–domain correlation between two time series and can highlight the common high-energy regions between the two series [29]. For two original time series $X = \{x_1, x_2, \cdots, x_n\}$ and $Y = \{y_1, y_2, \cdots, y_n\}$

Continuous Wavelet Transform is used to compute W_n^X and W_n^Y, and the cross wavelet power $W_n^{XY}(s)$ is calculated as follows:

$$W_X(T,S) = \int_{+\infty}^{-\infty} x(t) \cdot \psi_{T,S}^*(t)dt \quad (5)$$

In Equation (5), $W_n^Y(s)_*$ represents the complex conjugate of $W_n^Y(s)$, and S the fundamental deviation of the wavelet phase angle. A larger cross wavelet power indicates a stronger resonance between the two time series, showing a higher frequency correlation at that particular time scale.

Wavelet coherence can reflect the covariance strength between two time series in the time–frequency domain, and it has strong coverage for correlations in low-energy regions [30]. The wavelet coherence spectrum for two original time series $X = \{x_1, x_2, \cdots, x_n\}$ $Y = \{y_1, y_2, \cdots, y_n\}$ is defined as:

$$R_n^2(s) = \frac{\left|S(s^{-1}W_n^{XY}(s))\right|^2}{S(s^{-1}|W_n^X(s)|^2)S(s^{-1}|W_n^Y(s)|^2)} \quad (6)$$

In Equation (6), S represents the smoothing operator, and S^{-1} denotes the inverse smoothing transform. $W_n^{XY}(s)$ is the cross wavelet power. The wavelet coherence value R^2 ranges between 0 and 1, and can be regarded as the local correlation coefficient at a given time–frequency. A higher value indicates a stronger frequency correlation between the two time series at that specific time scale.

2.3.4. Correlation Analysis Method

Pearson correlation analysis is used to examine the strength and direction of the linear relationship between two sets of variables [31]. A correlation coefficient close to 1 indicates a strong positive correlation between the variables, while a value close to -1 indicates a strong negative correlation. The calculations were performed using the "corr.test()" function from the psych package built into R version 4.2.3. The visualization of the correlation matrix was performed using the corrplot package [32].

3. Results

3.1. Spatial Variation Characteristics of Heavy Rainfall in the Taihang Mountains Based on REOF Partitioning

The annual heavy rainfall data from 13 stations, spanning the past 50 years, were first normalized and then subjected to EOF decomposition. Subsequently, the principal components underwent maximum orthogonal variance rotation to derive the REOF decomposition results [33]. The EOF and REOF decomposition results are shown in Table 2. Typically, an EOF cumulative variance contribution rate of 85% is used as the criterion for determining the number of REOF eigenvectors [34]. Accordingly, the first six eigenmodes were selected for analysis. ArcGIS (Version 10.8). was utilized to plot the REOF loading vector distribution maps for these six modes (Figure 2). Based on the high-value areas of the loading vectors, a schematic diagram illustrating the heavy rainfall partitions in the Taihang Mountains was produced (Figure 3).

Table 2. Variance and cumulative contributions of EOF and REOF decomposition.

Serial Number	EOF		REOF	
	Variance Contribution%	Cumulative Variance Contribution%	Variance Contribution%	Cumulative Variance Contribution%
1	41.63	41.63	18.01	18.01
2	14.27	55.90	13.65	31.66
3	11.64	67.54	13.60	45.26
4	9.12	76.67	11.14	56.40
5	6.03	82.69	11.08	67.49
6	4.77	87.47	9.58	77.07

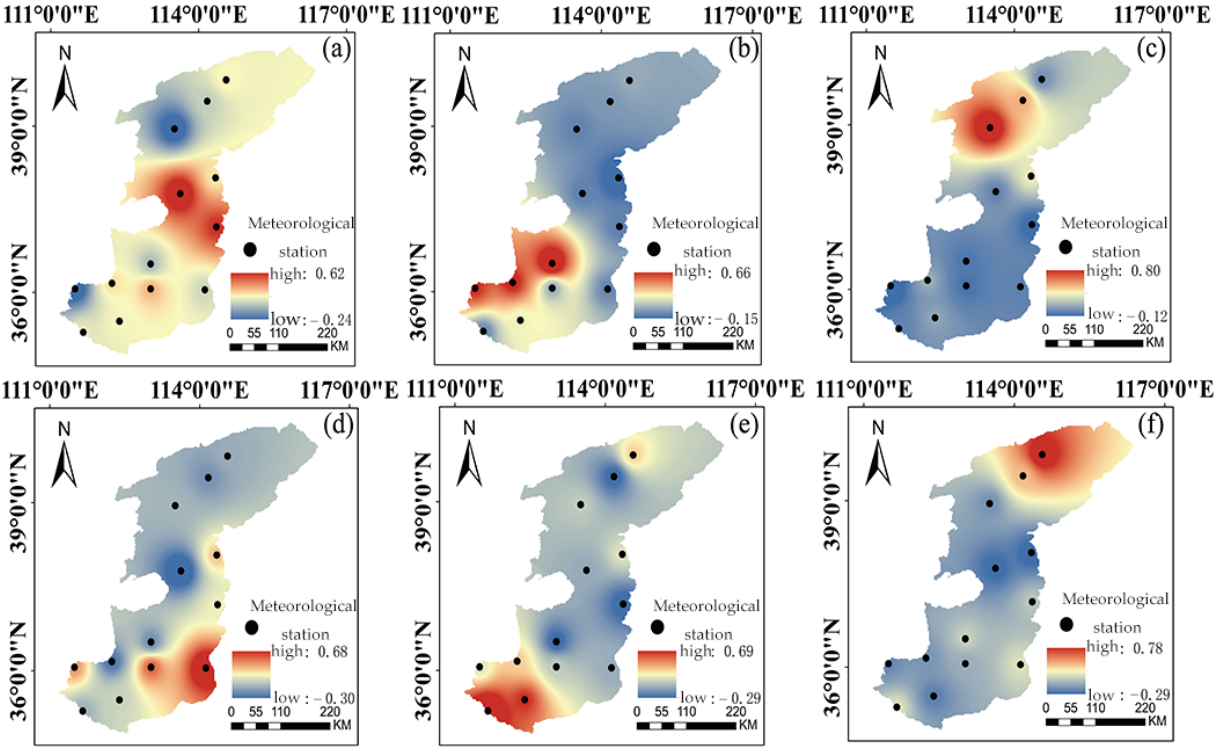

Figure 2. Spatial distribution of modal values in the six partitions of the Taihang Mountains. (**a**–**f**) Represent the spatial distribution of modal values for Partitions I to VI, respectively.

As illustrated in Figure 3, Region I is situated in the central Taihang Mountains, within the transition zone between the plains and the mountains. It predominantly covers the Pingding and Xingtai areas, comprising 17% of the total area of the Taihang Mountains. This region experiences a warm temperate sub-humid monsoon climate, characterized by distinct seasons and concentrated rainfall. The windward slope terrain significantly contributes to the higher annual heavy rainfall in this area. Region II is located on the leeward slope in the southern Taihang Mountains, encompassing the Linfen, Anze, and Xiangyuan areas, and covers 26% of the total area. This region experiences relatively less heavy rainfall. Region III is positioned in the northwestern Taihang Mountains, primarily covering the Wutai Mountain, Lingqiu, and Shijiazhuang areas, and spans 26% of the total area. This region lies in the transition zone between a temperate monsoon climate and a temperate continental climate, resulting in relatively low annual heavy rainfall. Region IV is located in the southeastern Taihang Mountains, within the transition zone from the plains to the hilly terrain, primarily including the Changzhi and Anyang areas, and covering 14% of the total area. This region experiences a warm temperate continental monsoon climate [35], where the summer monsoon is uplifted by the terrain, often leading to heavy rainfall. Consequently, this region records the highest annual heavy rainfall [36]. Region

V is situated in the southern Taihang Mountains, within the Jin-South Guanzhong Basin, covering the Yuanqu and Yangcheng areas, and accounting for 8% of the total area. The funnel-shaped terrain and the narrowing landscape force the convergence and uplift of the airflow, which easily triggers strong rainfall events [37]. Region VI is positioned in the northernmost Taihang Mountains, within the hilly region of North China, primarily encompassing Yu County, and covering 17% of the total area. This region experiences a temperate continental monsoon climate and receives the least annual heavy rainfall.

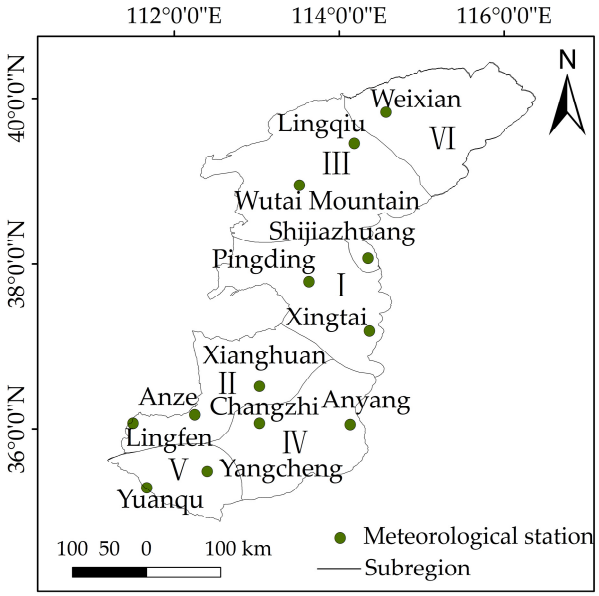

Figure 3. Schematic diagram of heavy rainfall geographic partitioning in the Taihang Mountains.

3.2. Interannual Variation Trends of Heavy Rainfall in the Six Partitions of the Taihang Mountains

This study employed linear regression analysis and the Mann–Kendall (MK) trend test to evaluate the interannual variation trends of heavy rainfall across six partitions in the Taihang Mountains (Figure 4). The results indicate that, although heavy rainfall fluctuated significantly in each partition during the study period, the overall trend shows an increase ($R^2 > 0$, $Z > 0$). In Partition I, heavy rainfall peaked at 307.4 mm in 2016, with an average increase of approximately 4 mm per decade. In Partition II, heavy rainfall peaked at 201 mm in 2013, with an average increase of 14.4 mm per decade. This upward trend passed the 95% significance test ($p < 0.05$), indicating statistical significance. In Partition III, heavy rainfall reached its highest value of 310.5 mm in 1996, with an average increase of around 4.7 mm per decade. In Partition IV, heavy rainfall peaked at 726 mm in 2021, with an average increase of 15.1 mm per decade. This extreme value greatly exceeded those in other partitions, suggesting that the funnel-shaped topography in this region is more sensitive to short-duration rainfall as precipitation intensity increases [38]. In Partition V, heavy rainfall peaked at 387.7 mm in 1982, with an average increase of 8.7 mm per decade.

In Partition VI, heavy rainfall peaked at 66.1 mm in 1991, with an average increase of 0.5 mm per decade. Overall, the interannual variation trends in heavy rainfall across all partitions exhibit an upward tendency, reflecting the influence of local climate change on the characteristics of heavy rainfall.

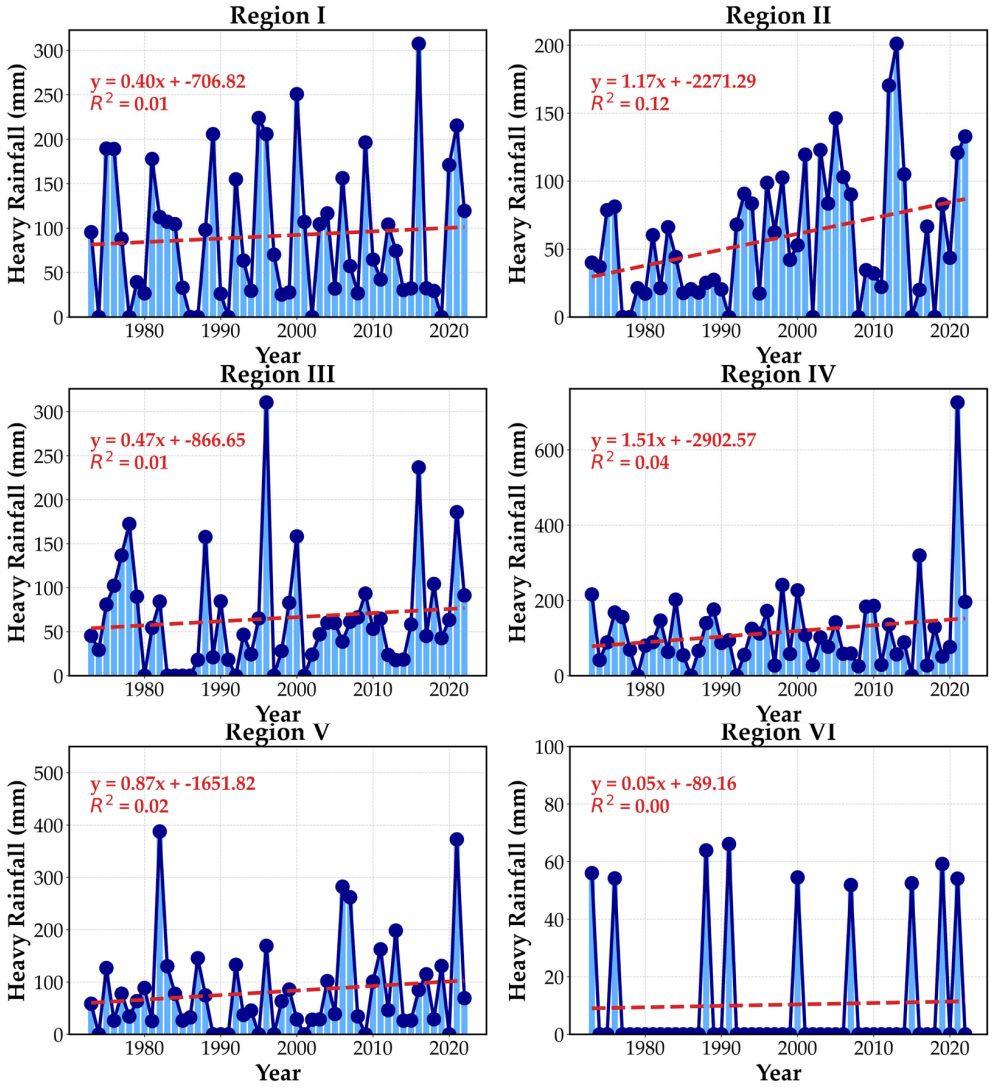

Figure 4. Interannual variation in heavy rainfall in six partitions of the Taihang Mountains from 1973 to 2022.

3.3. Temporal Variation Characteristics of Heavy Rainfall in the Taihang Mountains Based on REOF Partitioning

To investigate the temporal variation characteristics of heavy rainfall in the six partitions of the Taihang Mountains, this study applied the Continuous Wavelet Transform power spectrum to analyze heavy rainfall conditions across these partitions from 1973 to 2022 (Figure 5). In Region I, clear oscillations are observed with periods of 2–4 years, 3–5 years, and 6–7 years [see Figure 5a]. In Region II, significant oscillations occur with periods of 2–3 years, 3–5 years, and 5–9 years [see Figure 5b]. In Region III, a prominent oscillation period of 2.5–5 years is evident [see Figure 5c]. In Region IV, a significant oscillation period of 2.5–3 years is apparent [see Figure 5d]. In Region V, heavy rainfall demonstrates an oscillation period of 4.5–5.5 years [see Figure 5e]. In Region VI, heavy rainfall shows a periodic variation of 2.5–3.5 years [see Figure 5f]. The Continuous Wavelet Transform results indicate that all six heavy rainfall partitions over the past 50 years exhibit oscillation periods of approximately 2–3 years. According to related studies, summer precipitation in regions such as South China, North China, and the Yangtze River Basin also exhibit periodic scales of 2–3 years. This oscillation, known as the quasi-biennial oscillation (QBO) [39], suggests that the QBO characteristics of the East Asian summer monsoon may influence the periodicity of heavy rainfall in the Taihang Mountains region.

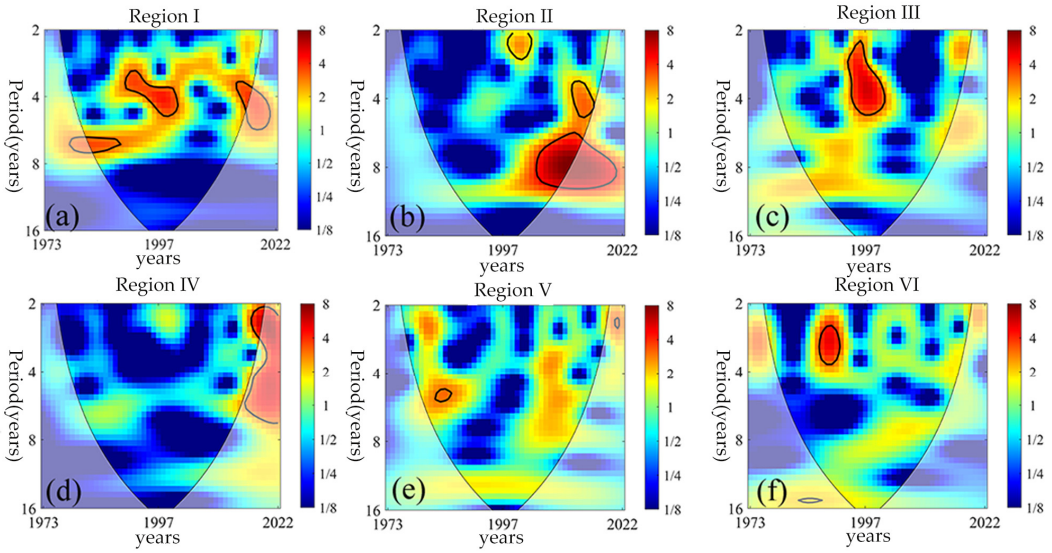

Figure 5. Continuous Wavelet Transform diagrams for each partition in the Taihang Mountains. Note: The black solid-lined areas indicate regions passing the 95% red noise test, and the white cone-shaped areas represent the cone of influence due to boundary effects.

3.4. Relationship Between Heavy Rainfall in Each Partition and Large-Scale Circulation

Based on relevant studies surrounding the research area [40–43], eight circulation factors—NAO, PDO, AO, SOI, WP, NP, IOD, and PWR—were selected to analyze their influence on heavy rainfall in each partition of the Taihang Mountains. As shown in Figure 6, the correlation coefficients between heavy rainfall in Region I and SOI and IOD passed the 90% significance test. Region I exhibits a positive correlation with SOI ($p < 0.1$) and a negative correlation with IOD ($p < 0.1$). The correlation coefficients between heavy rainfall in Region II and PDO and PWR passed the 90% significance test. Region II shows a negative correlation with PDO ($p < 0.1$) and a positive correlation with PWR ($p < 0.1$). The correlation coefficient between heavy rainfall in Region III and SOI passed the 95% significance test, showing a positive correlation ($p < 0.05$). The correlation coefficient between heavy rainfall in Region IV and PDO passed the 90% significance test, while the coefficients with SOI and PWR passed the 95% significance test. Region IV is negatively correlated with PDO ($p < 0.1$) and positively correlated with SOI and PWR ($p < 0.05$). Regions V and VI did not show any significant correlations with the circulation factors.

Building on the correlation analysis (Figure 6), Cross Wavelet Transform (XWT) and Wavelet Coherence (WTC) analyses were performed to further investigate the relationships between significant circulation factors and the identified regions (Figures 7 and 8) [44]. Significant resonance periods were identified between heavy rainfall in Region I and the circulation factors SOI and IOD in both high- and low-energy regions. In the high-energy region, resonance periods of 3–4 years and 3–5 years are observed between heavy rainfall in Region I and SOI [see Figure 7a]. In the low-energy region, resonance periods of 2–3 years, 3.5–5 years, and 3–6 years are present [see Figure 8a]. The phase relationship reveals that changes in SOI lead changes in heavy rainfall in Region I, and they are in positive phase alignment. In the high-energy region, resonance periods of 3–5 years and 3.5–4 years are detected between heavy rainfall in Region I and IOD [see Figure 7b]. In the low-energy region, resonance periods of 12–16 years and 2–3 years are evident [see Figure 8b]. The phase relationship indicates that changes in the IOD index lag behind changes in heavy rainfall in Region I, and they exhibit negative phase alignment.

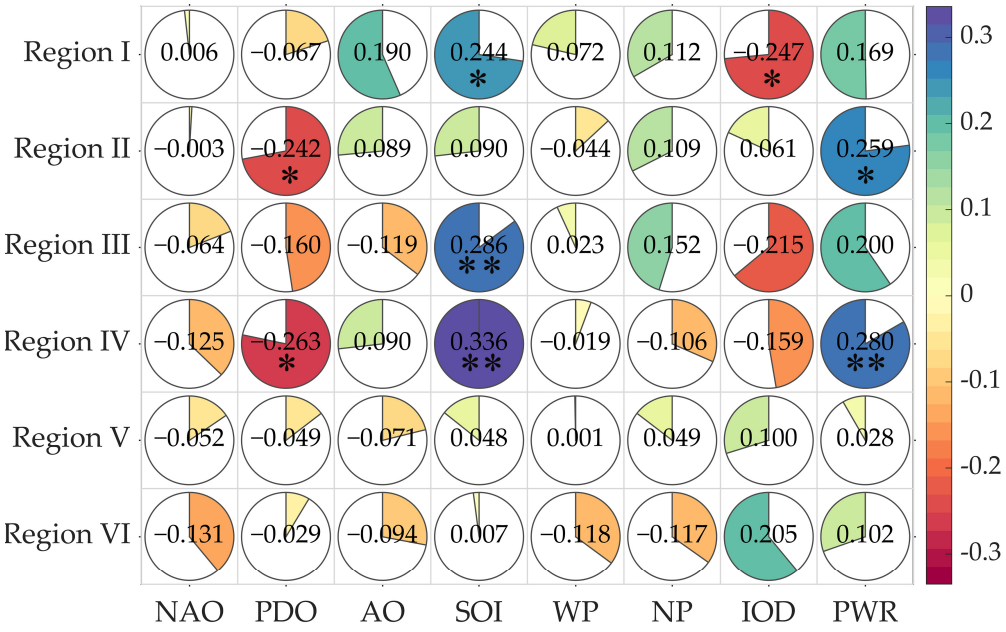

Figure 6. Heatmap of correlation between partitioned heavy rainfall and circulation factors. Note: The symbols **, and * indicate significance levels at 0.05, and 0.1, respectively.

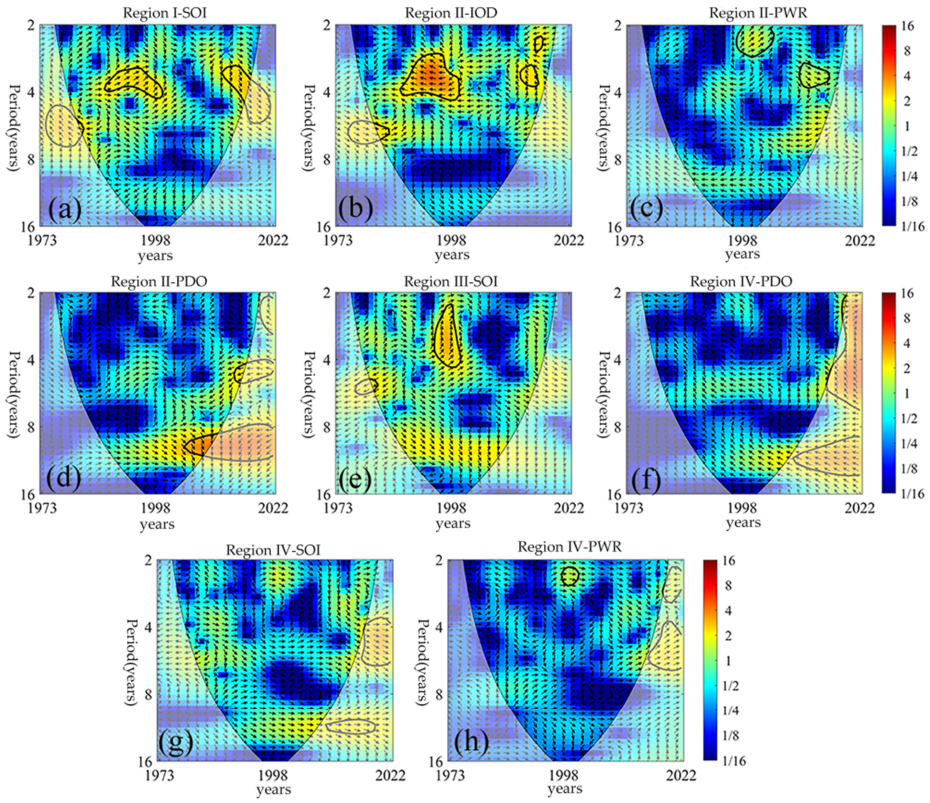

Figure 7. Cross wavelet analysis diagram of Taihang Mountain partitions and circulation factors. Note: The black solid-lined areas indicate regions passing the 95% significance test. Higher values represent stronger correlations between the two. Rightward arrows indicate a positive correlation between partitioned heavy rainfall and circulation factors, leftward arrows indicate a negative correlation, and upward or downward arrows indicate whether heavy rainfall lags or leads the circulation factor by 1/4 phase.

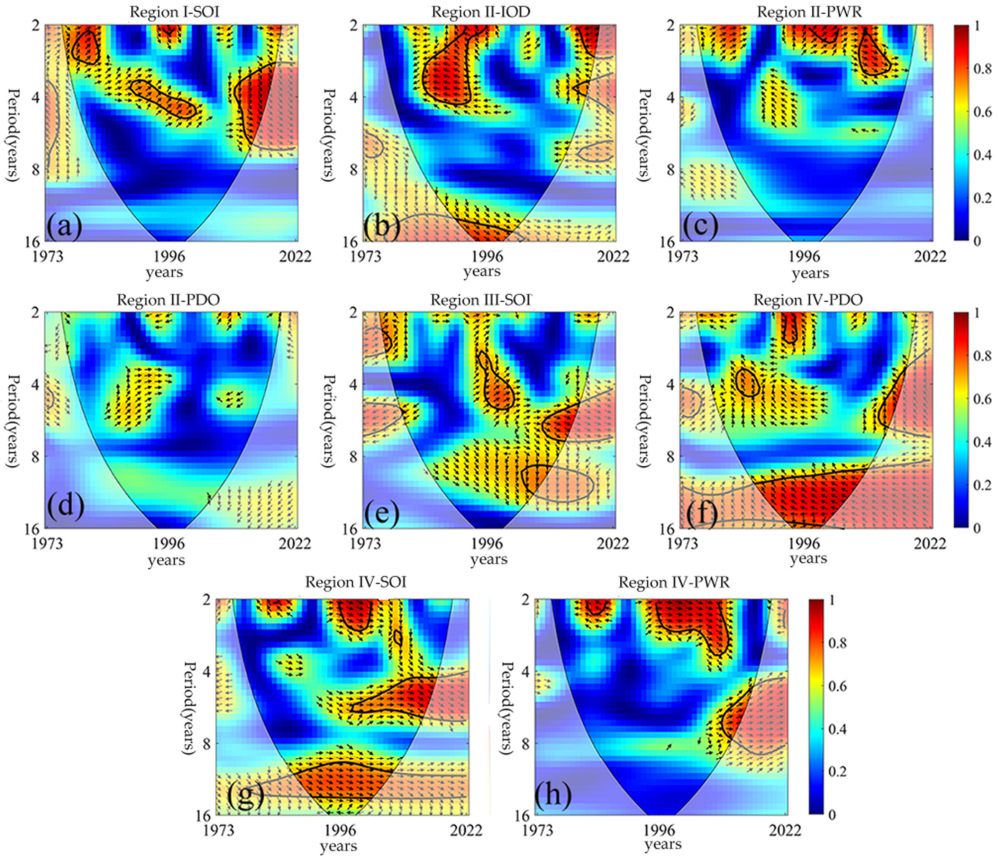

Figure 8. Wavelet coherence analysis diagram of Taihang Mountain partitions and circulation factors.

In Region II, resonance periods between heavy rainfall and the PWR circulation factor are detected in both high- and low-energy regions. In the high-energy region, there is a resonance period of 1–4 years between heavy rainfall and PWR [see Figure 7c], while a shorter oscillation period of 2–3 years is observed in the low-energy region [see Figure 8c]. The phase relationship indicates that PWR changes lead heavy rainfall in Region II, with the two remaining in positive phase alignment. Additionally, a resonance period of 8–10 years is identified between heavy rainfall and the PDO in the high-energy region [see Figure 7d], where PDO changes precede heavy rainfall by approximately 1/4 phase. However, no resonance period is observed between heavy rainfall and PDO in the low-energy region [see Figure 8d].

In Region III, significant resonance periods are also observed between heavy rainfall and the SOI circulation factor. In the high-energy region, the resonance period with SOI is 2–5 years [see Figure 7e]. In the low-energy region, the resonance periods range from 3–5 years and 5–8 years [see Figure 8e]. The phase relationship shows that SOI changes precede heavy rainfall in Region III, with the two in positive phase alignment.

In Region IV, significant resonance periods are detected between heavy rainfall and the PDO and SOI circulation factors in the low-energy region, while no resonance periods are observed in the high-energy region [Figure 7f,g]. In the low-energy region, a resonance period of 12–16 years is observed between heavy rainfall in Region IV and PDO [Figure 8f]. The phase relationship indicates that PDO changes lag behind heavy rainfall changes in Region IV, with a predominantly negative phase alignment. Resonance periods of 10–14 years and 4–7 years are observed in the low-energy region between heavy rainfall in Region IV and SOI [Figure 8g]. The phase relationship shows that SOI changes precede heavy rainfall changes in Region IV, with a predominantly positive phase alignment. Significant resonance periods are detected between heavy rainfall in Region IV and the PWR circulation factor in both high- and low-energy regions. In the high-energy region, a resonance period of 2–3 years is identified [Figure 7h], while in the low-energy region,

resonance periods of 1–2 years, 2–3 years, and 4–8 years are present [Figure 8h]. The phase relationship indicates that PWR changes precede heavy rainfall changes in Region IV, with a predominantly positive phase alignment.

4. Discussion

Using the MK trend test and linear fitting analysis, this study reveals that heavy rainfall in all regions of the Taihang Mountains exhibited an increasing trend from 1973 to 2022. This trend is likely closely related to global warming, which accelerates the water cycle. In particular, with increased monsoon intensity, both the frequency and intensity of precipitation in eastern and southern China have risen significantly [45,46]. Additionally, periodic fluctuations of approximately 2–3 years were observed in heavy rainfall across different regions during certain periods. This short-term periodicity was reflected in the linear fitting analysis and matched the periodicity derived from Continuous Wavelet Transform (CWT) results. The CWT results indicated that, under the influence of the quasi-biennial oscillation (QBO), heavy rainfall in each region exhibited periodic variations on a 2–3 year timescale. This implies that, besides the long-term increasing trend, regional rainfall also experiences regular short-term oscillations. These findings suggest that the likelihood of future heavy rainfall events in the Taihang Mountains is likely to increase, consistent with the results reported by Jie Ban et al. Therefore, it is imperative to enhance storm warning systems and strengthen flood control infrastructure [47] to mitigate the potential risks posed by frequent heavy rainfall. Due to the fluctuations in the time series, the M–K trend test employed in this study may be influenced by the scaling hypothesis to some extent [48]. Zichen Hu et al. refined the M–K trend test based on the scaling hypothesis [49], leading to more reliable outcomes. Future studies may consider adopting the improved M–K method to derive more robust conclusions.

Of the six heavy rainfall regions in the Taihang Mountains, regions I, III, and IV are situated in the transition zone between the North China Plain and the eastern mountainous and hilly areas of the Taihang Mountains. Heavy rainfall in these three regions is positively correlated with the Southern Oscillation Index (SOI). Li Fen et al. highlighted that changes in SOI significantly affect precipitation in northern Jinzhong, a part of the southern region of the study area, showing a similar positive correlation [50]. A strong SOI is commonly associated with La Niña events. When sea surface temperatures in the Indonesian region are elevated and atmospheric pressure is low, the southeast monsoon over China intensifies [51], shifting the primary rainfall zone northward [52] and increasing rainfall in northern China. During this process, the elevation of the Taihang Mountains increases gradually from the eastern plains to the western mountains, particularly in regions I and IV. The sharp topographic changes cause uplift in airflows, making these areas more prone to concentrated heavy rainfall during periods of intensified southeast monsoons [53]. Furthermore, land use types in these areas influence runoff patterns after heavy rainfall, further shaping the spatial distribution characteristics of rainstorms. Heavy rainfall in regions II and IV is positively correlated with the Pacific Warm Pool Index (PWR) and negatively correlated with the Pacific Decadal Oscillation (PDO). When sea surface temperatures in the Pacific Warm Pool rise abnormally, the subtropical high-pressure ridge shifts northward, leading to a stronger summer monsoon [54]. As a result, the rain belt lingers longer over northern China, increasing the frequency of summer storms in these regions. When the PDO is in its negative phase, temperatures in the North China Plain tend to be relatively low, and atmospheric pressure is no longer abnormally high. Concurrently, the influence of anomalous northwesterly winds weakens, enabling smoother moisture transport [55]. The negative phase of the PDO makes regions II and IV more susceptible to heavy rainfall events. Additionally, differences in land use types (e.g., urbanized areas vs. farmland) may further influence the hydrological response in these regions. Heavy rainfall in region I is negatively correlated with the Indian Ocean Dipole (IOD). Research indicates that during positive IOD years, summer rainfall increases south of the Yangtze River, particularly in Jiangxi and Hunan, while it decreases north of the Yangtze River [56]. During negative

IOD years, the Walker circulation over the Indian Ocean strengthens, while it weakens over the Pacific [57], leading to reduced precipitation in the western Pacific and, subsequently, decreased rainfall in northern China. The fluctuations in the Indian Ocean Dipole (IOD) are negatively correlated with summer rainfall in northern China, consistent with the findings of this study. Variations in these circulation indices provide critical insights into the distribution patterns of heavy rainfall in the Taihang Mountains. Integrating SOI, IOD, PWR, and PDO into future storm forecasting models for the Taihang Mountains is expected to enhance the accuracy of heavy rainfall predictions, offering valuable insights for disaster prevention, mitigation, and protecting people's livelihoods and safety.

Previous studies on heavy rainfall in the Taihang Mountains have predominantly focused on numerical simulations of specific storm events and basic analyses of the spatiotemporal distribution of rainfall using the Empirical Orthogonal Function (EOF) model. Compared to the EOF method, the Rotated Empirical Orthogonal Function (REOF) method more effectively reveals the geographical characteristics of different spatial fields and has become a growing trend in the separation of climate vector fields [58]. The complex topography and circulation patterns in the Taihang Mountains necessitate the use of the REOF method to partition heavy rainfall regions, along with Pearson correlation analysis to explore the relationships between rainfall and circulation factors. China's primary climate zoning divides the country into five trend zones based on temperature and precipitation trends, while secondary zoning categorizes the country into 14 zones based on temperature and precipitation fluctuation characteristics [59]. In this study, the boundaries of partitions III and IV, along with those of partitions I, II, and III, align closely with the I3, I2, and I4 subzones of China's secondary climate zoning. This indicates that the REOF method for partitioning heavy rainfall in the Taihang Mountains is highly reliable. However, the occurrence of heavy rainfall results from the combined effects of multiple factors. This study only considered the influence of individual factors on heavy rainfall, neglecting the complex interactions and interdependencies among various factors. Future research could apply machine learning to investigate the importance of multiple factors in assessing heavy rainfall. Furthermore, the impact of human activities on heavy rainfall should also be considered, including land use changes, global warming driven by human actions, and the effects of water resource management and flood control projects on the occurrence of heavy rainfall.

5. Conclusions

This study, based on precipitation data from 13 meteorological stations in the Taihang Mountains from 1973 to 2022, identified rainstorms using a 50 mm precipitation threshold. Multiple methods, including REOF analysis, linear fitting, the MK trend test, Continuous Wavelet Transform (CWT), Cross Wavelet Transform (XWT), Wavelet Coherence (WTC), and Pearson correlation analysis, were utilized to investigate the spatiotemporal distribution of rainstorms in the Taihang Mountains over the past 50 years and the large-scale climate factors affecting rainstorms in each partition. The key conclusions are as follows:

(1) Spatial heterogeneity: The REOF analysis divided the Taihang Mountains into six distinct rainstorm partitions, each showing spatial heterogeneity in rainfall distribution. Partition I, located in the transition zone between the plains and mountains in the central region, experiences relatively higher rainfall due to orographic uplift. Partition IV, situated in the southeast, records the highest rainfall, driven by significant monsoon uplift during the summer. In contrast, partitions III and VI have lower rainfall, with partition VI, located in the northern hilly region, having the least rainfall. These spatial differences in rainstorm distribution are closely linked to the region's complex terrain and climatic patterns.

(2) Interannual variation trends: Over the past 50 years, rainfall in each partition of the Taihang Mountains has shown an increasing trend. Partition II displayed a significant upward trend ($p < 0.05$), with rainfall increasing at a rate of 14.4 mm per decade. This trend is closely related to the intensification of the water cycle under global warming,

highlighting the impact of climate change on the frequency and intensity of regional rainstorms.

(3) Periodicity: Results from the Continuous Wavelet Transform revealed significant 2–3-year periodic fluctuations in rainfall across all partitions. This periodicity aligns with the quasi-biennial oscillation (QBO) characteristics of the East Asian Summer Monsoon. The study found that all six rainstorm partitions experienced oscillation cycles of approximately 2–3 years over the past 50 years, indicating that QBO characteristics of the East Asian Summer Monsoon influence rainfall periodicity in the Taihang Mountains. This periodic pattern provides valuable reference information for future climate forecasting.

(4) Influence of large-scale circulation factors: Correlation and wavelet resonance analyses revealed that rainfall in Partitions II, III, and IV is positively correlated with the Southern Oscillation Index (SOI), while rainfall in Partitions II and IV is positively correlated with the Pacific Warm Pool Region (PWR) and negatively correlated with the Pacific Decadal Oscillation (PDO). Rainfall in Partition I is negatively correlated with the Indian Ocean Dipole (IOD). These variations in large-scale circulation factors not only influence the frequency of rainstorms but are also linked to the temporal lag of rainstorm events. Incorporating these factors into future rainstorm prediction models is expected to enhance the accuracy of rainstorm forecasting.

The REOF method, Continuous Wavelet Transform, and correlation analysis used in this study have shown strong applicability for studying rainstorms in the Taihang Mountains and have broad potential for wider application. These methods are particularly suitable for other regions with complex terrain and climatic conditions, especially areas where mountainous or monsoonal climates play a significant role. For instance, in the southwestern mountainous areas, the Tibetan Plateau, and other global monsoon regions, these methods could be used to study the spatial distribution of extreme precipitation events and the interaction of climatic factors. Moreover, these analytical techniques can be applied in other climate and environmental fields, such as flood forecasting and disaster management, offering more precise and efficient tools.

This study is the first to apply the REOF method for fine spatial partitioning of rainstorms in the Taihang Mountains, combined with resonance analysis of large-scale climate factors. It reveals the complex spatiotemporal relationships between rainfall and circulation factors. This multi-scale analytical approach provides new insights into improving rainstorm prediction models and contributes to enhancing the accuracy of extreme weather forecasting.

Author Contributions: Conceptualization, Q.T. and Z.F.; methodology, Q.T.; software, Z.F. and Y.M.; formal analysis, Z.F.; investigation, Q.T., Z.F. and Y.L.; resources, Q.T.; data curation, J.X., M.H. and Y.L.; writing—original draft preparation, Q.T.; writing—review and editing, W.Z.; visualization, Z.F. and Y.M.; project administration, Q.T.; funding acquisition, Q.T. All authors have read and agreed to the published version of the manuscript.

Funding: This research was financially supported by the following projects: Henan Province Science and Technology Key Project (Grant Nos. 242102320016 and 232102321109); Henan Province Xingwenhua Project Cultural Research Special (Grant No. 2023XWH020); Henan Province Key Research Project of Higher Education Institutions (Grant No. 24A170003); Anyang National Climate Observatory Open Research Fund (Grant No. AYNCOF202311); Science and Technology Research Project of Anyang City (Grant No. 2023C01SF133); Key Scientific Research Project of Colleges and Universities in Henan Province (Grant No. 24A170002); and Foundation for Distinguished Young Talents in Higher Education of Henan (Grant No. 2023GGJS125).

Data Availability Statement: The data presented in this study are available on request from the first author.

Acknowledgments: We thank the Henan Provincial Department of Science and Technology, the Henan Provincial Department of Education, and the Anyang National Climate Observatory for their strong support of this project.

Conflicts of Interest: The authors declare no conflicts of interest.

References

1. Junior, F.D.C.V.; Zachariah, M.; do Vale Silva, T.L.; dos Santos, E.P.; Coelho, C.A.; Alves, L.M.; Martins, E.S.P.R.; Köberle, A.C.; Singh, R.; Vahlberg, M.; et al. An attribution study of very intense rainfall events in Eastern Northeast Brazil. *Weather Clim. Extrem.* **2024**, *45*, 100699.
2. Sene, K.; Sene, K. Flash floods. In *Hydrometeorology: Forecasting and Applications*; Springer: Berlin/Heidelberg, Germany, 2016; pp. 273–312.
3. Qin, W. Study on the Anomalous Characteristics and Causes of Heavy Rainfall Climate Change in Guangxi. Ph.D. Thesis, Nanjing University of Information Science & Technology, Nanjing, China, 2022.
4. Zhu, Y.H.; Ren, L.L.; Lü, H.S.; Zhang, Y.L. *Water Ecological Protection and Restoration*; China Water & Power Press: Beijing, China, 2020.
5. Wang, H.; Chen, B.; Shen, X. Extreme rainfall, farmer vulnerability, and labor mobility—Evidence from rural China. *Sci. Total Environ.* **2024**, *918*, 170866. [CrossRef] [PubMed]
6. Armah, F.A.; Yawson, D.O.; Yengoh, G.T.; Odoi, J.O.; Afrifa, E.K. Impact of floods on livelihoods and vulnerability of natural resource dependent communities in Northern Ghana. *Water* **2010**, *2*, 120–139. [CrossRef]
7. Cavalcante, L.; Walker, D.W.; Kchouk, S.; Ribeiro Neto, G.; Carvalho, T.M.N.; de Brito, M.M.; Pot, W.; Dewulf, A.; van Oel, P. From insufficient rainfall to livelihoods: Understanding the cascade of drought impacts and policy implications. *EGUsphere* **2024**, *2024*, 1–20.
8. Yan, G. Study on the Impact of the Taihang Mountains on Rainstorms in North China. Ph.D. Thesis, Nanjing University of Information Science & Technology, Nanjing, China, 2013.
9. Lin, H.; Min, J.; Zhu, L.; Xu, Y.; Tao, Y. The Role of Taihang Mountain Topography in the Persistent Low Vortex Rainstorm over North China on "7.19". *Meteorol. Sci.* **2023**, *1*, 46–58.
10. Li, Z.; Yang, H.; Jia, M. Factors Affecting the Spatiotemporal Variation of Precipitation in the Songhua River Basin of China. *Water* **2024**, *16*, 2. [CrossRef]
11. Kömüşcü, A.Ü.; Aksoy, M. Characterizing variability of spatial patterns of annual and seasonal precipitation of Turkey and identifying the probable driving factors including teleconnection patterns. *J. Water Clim. Change* **2024**, *15*, 1392–1416. [CrossRef]
12. Zeleke, T.T.; Lukwasa, A.Z.W.; Beketie, K.T.; Ayal, D.Y. Analysis of Spatio-Temporal Precipitation and Temperature Variability and Trend over Sudd-Wetland, Republic of South Sudan. *Clim. Serv.* **2024**, *34*, 100451. [CrossRef]
13. Stikeleather, W.D.; Roundy, P.E. Application of a Two-Step Space-Time EOF Statistical Postprocessing Algorithm to Mitigate Sub-Seasonal 200hPa Geopotential Height Forecast Error. *Weather Forecast.* **2024**. [CrossRef]
14. Chen, L.; Zhong, X.; Li, H.; Wu, J.; Lu, B.; Chen, D.; Xie, S.-P.; Wu, L.; Chao, Q.; Lin, C.; et al. A Machine Learning Model That Outperforms Conventional Global Subseasonal Forecast Models. *Nat. Commun.* **2024**, *15*, 6425. [CrossRef]
15. Hannachi, A.; Jolliffe, I.T.; Stephenson, D.B. Empirical orthogonal functions and related techniques in atmospheric science: A review. *Int. J. Climatol.* **2007**, *27*, 1119–1152. [CrossRef]
16. Gao, H.; Fu, T.; Liu, J.; Liang, H.; Han, L. Ecosystem Services Management Based on Differentiation and Regionalization along Vertical Gradient in Taihang Mountain, China. *Sustainability* **2018**, *10*, 986. [CrossRef]
17. Fu, T.; Gao, H.; Liang, H.; Liu, J. Spatio-Temporal Precipitation Changes and Their Localized Predictors in the Taihang Mountain Region, North China. *Stoch. Environ. Res. Risk Assess.* **2021**, *35*, 665–679. [CrossRef]
18. Chen, X.; Zou, X.; Zhang, Q. *Rainstorm Disaster Grade (GB/T 33680-2017)*; China Standards Press: Beijing, China, 2017.
19. Rodrigues, D.T.; Gonçalves, W.A.; Spyrides, M.H.C.; Andrade, L.M.B.; Souza, D.O.; Araujo, P.A.A.; Silva, A.C.N.; Santos e Silva, C.M. Probability of Occurrence of Extreme Precipitation Events and Natural Disasters in the City of Natal, Brazil. *Urban Clim.* **2021**, *35*, 100753. [CrossRef]
20. Springer, S.; Laio, A.; Galfi, V.M.; Lucarini, V. Unsupervised Detection of Large-Scale Weather Patterns in the Northern Hemisphere via Markov State Modelling: From Blockings to Teleconnections. *Npj Clim. Atmos. Sci.* **2024**, *7*, 105. [CrossRef]
21. Blumenauer, E. Examining the Vertical Structure of Hurricane Laura (2020) Using Azimuthal-Mean Vertical Profiles and an EOF Analysis. 2023. Available online: https://hdl.handle.net/11244/337944 (accessed on 27 October 2024).
22. Khoir, A.N.; Ooi, M.C.; Juneng, L.; Ramadhan, M.A.; Virgianto, R.H.; Tangang, F. Spatio-Temporal Analysis of Aerosol Optical Depth Using Rotated Empirical Orthogonal Function over the Maritime Continent from 2001 to 2020. *Atmos. Environ.* **2022**, *290*, 119356. [CrossRef]
23. Chang, C.H.; Lee, H.; Do, S.K.; Du, T.L.; Markert, K.; Hossain, F.; Ahmad, S.K.; Piman, T.; Meechaiya, C.; Bui, D.D.; et al. Operational Forecasting Inundation Extents using REOF analysis (FIER) over Lower Mekong and its Economic Impact on Agriculture. *Environ. Model. Softw.* **2023**, *162*, 20230014033. [CrossRef]
24. Çelebioğlu, T.; Tayanç, M. A Study on Precipitation Trends in Türkiye via Linear Regression Analysis and Non-Parametric Mann-Kendall Test. *Sürdürülebilir Çevre Derg.* **2024**, *4*, 19–28. [CrossRef]
25. Gowthaman, T.; Kumar, S.; Bhattacharyya, B. Detecting air pollutants trends using Mann-Kendall tests and Sen's slope estimates. *Environ. Conserv. J.* **2023**, *24*, 157–166.
26. Mondal, C.; Uddin, M.J. Assessment of climate change induced rainfall trend and variability with non-parametric and linear approach for Sirajganj district, Bangladesh. *Heliyon* **2024**, *10*, e31151. [CrossRef]

27. Magrini, L.A.; Oliveira Domingues, M.; Macau, E.E.N.; Kiss, I.Z. Extraction of Slow and Fast Dynamics of Multiple Time Scale Systems Using Wavelet Techniques. *Chaos Interdiscip. J. Nonlinear Sci.* **2020**, *30*, 063139. [CrossRef] [PubMed]
28. Priyadarshini, M.S.; Bajaj, M.; Prokop, L.; Berhanuz, M. Perception of Power Quality Disturbances Using Fourier, Short-Time Fourier, Continuous and Discrete Wavelet Transforms. *Sci. Rep.* **2024**, *14*, 3443. [CrossRef] [PubMed]
29. Knight, M.I.; Nunes, M.A.; Hargreaves, J.K. Adaptive wavelet domain principal component analysis for nonstationary time series. *J. Comput. Graph. Stat.* **2024**, *33*, 941–954. [CrossRef]
30. Sirohiwal, A.; Berraud-Pache, R.; Neese, F.; Izsák, R.; Pantazis, D.A. Accurate Computation of the Absorption Spectrum of Chlorophyll a with Pair Natural Orbital Coupled Cluster Methods. *J. Phys. Chem. B* **2020**, *124*, 8761–8771. [CrossRef]
31. Allega, L. Variaciones de la Temperatura del Mar y Sus Efectos en Las Pesquerías en Un Área de Interés Estratégico del Mar Argentino. Ph.D. Thesis, Universidad Nacional del Sur, Bahía Blanca, Argentina, 2022.
32. Hansani, K.; Thilakarathne, E.; Koongolla, J.B.; Gunathilaka, W.; Perera, B.; Weerasingha, W.; Egodauyana, K. Contamination of Microplastics in Tropical Coral Reef Ecosystems of Sri Lanka. *Mar. Pollut. Bull.* **2023**, *194*, 115299. [CrossRef]
33. Cretignier, M.; Dumusque, X.; Pepe, F. Stellar activity correction using PCA decomposition of shells. *Astron. Astrophys.* **2022**, *659*, A68. [CrossRef]
34. Basnayake, B.M.L.A. Rainfall regimes in Sri Lanka. *Hydrol. Sci. J.* **2023**, *68*, 585–603. [CrossRef]
35. Qu, Q.; Jian, S.; Chen, A. Xiao, C. Investigating the Dynamic Change and Driving Force of Vegetation Carbon Sink in Taihang Mountain, China. *Land* **2024**, *13*, 1348. [CrossRef]
36. Cao, D. The Loess Highland in a Trading Network (1300–1050 BC). Ph.D. Thesis, Princeton University, Princeton, NJ, USA, 2014.
37. Wei, F. *Modern Climate Statistical Diagnosis and Forecasting Techniques*; Meteorological Press: Beijing, China, 2022.
38. Tang, Q.; Li, Y.; Hu, M.; Zhang, J.; Li, H.; Fu, Z.; Huang, S.; Li, Y. Analysis of the Spatiotemporal Evolution Characteristics of Rainstorms in the Taihang Mountains from 1973 to 2022. *J. Xinyang Norm. Univ. (Nat. Sci. Ed.)* **2024**, *37*, 524–531.
39. Han, J.; Fang, S.; Wang, X.; Zhuo, W.; Yu, Y.; Peng, X.; Zhang, Y. The Impact of Intra-Annual Temperature Fluctuations on Agricultural Temperature Extreme Events and Attribution Analysis in Mainland China. *Sci. Total Environ.* **2024**, *949*, 174904. [CrossRef]
40. Wang, T.; Song, C.; Chen, X. Clarifying the relationship between annual maximum daily precipitation and climate variables by wavelet analysis. *Atmos. Res.* **2023**, *295*, 106981. [CrossRef]
41. Wang, F.; Lai, H.; Li, Y.; Feng, K.; Tian, Q.; Zhang, Z.; Di, D.; Yang, H. Terrestrial Ecological Drought Dynamics and Its Response to Atmospheric Circulation Factors in the North China Plain. *Atmos. Res.* **2023**, *294*, 106944. [CrossRef]
42. Ling, M.; Guo, X.; Zhang, Y.; Yu, L.; Xi, Q. Drought Evolution in the Haihe River Basin During 1960–2020 and the Correlation with Global Warming, Sunspots, and Atmospheric Circulation Indices. *J. Water Clim. Change* **2023**, *14*, 369–386. [CrossRef]
43. Li, T.; Lv, A.; Zhang, W.; Liu, Y. Spatiotemporal Characteristics of Watershed Warming and Wetting: The Response to Atmospheric Circulation in Arid Areas of Northwest China. *Atmosphere* **2023**, *14*, 151. [CrossRef]
44. Polanco-Martínez, J.M.; Fernández-Macho, J.; Medina-Elizalde, M. Dynamic wavelet correlation analysis for multivariate climate time series. *Sci. Rep.* **2020**, *10*, 21277. [CrossRef]
45. Yi, P.; Chen, G.; Tang, X. Present and future climate of the Yangtze River Delta region: Analysis of the CMIP6 HighResMIP simulations. *Theor. Appl. Climatol.* **2024**, *155*, 8909–8921. [CrossRef]
46. Ban, J.; Lu, K.; Liu, Y.; Zang, J.; Zhou, Z.; Zhang, C.; Liu, Z.; Huang, J.; Chen, Y.; Gao, X.; et al. Projecting Future Excess Deaths Associated with Extreme Precipitation Events in China Under Changing Climate: An Integrated Modelling Study. *Lancet Planet. Health* **2024**, *8*, e723–e733. [CrossRef]
47. García Bu Bucogen, G. Estimación del Riesgo Asociado a la Ocurrencia de Inundaciones en La Cuenca Hidrográfica Inferior del río Negro (Argentina). Ph.D. Thesis, Universidad Nacional del Sur, Bahía Blanca, Argentina, 2023.
48. Shen, L.; Wen, J.; Zhang, Y.; Ullah, S.; Cheng, J.; Meng, X. Changes in Population Exposure to Extreme Precipitation in the Yangtze River Delta, China. *Clim. Serv.* **2022**, *27*, 100317. [CrossRef]
49. Hu, Z.; Liu, S.; Zhong, G.; Lin, H.; Zho, Z. Modified Mann-Kendall Trend Test for Hydrological Time Series Under the Scaling Hypothesis and Its Application. *Hydrol. Sci. J.* **2020**, *65*, 2419–2438. [CrossRef]
50. Li, F.; Zhang, Y.; Qiao, Y. Response of Seasonal Droughts and Floods in Shanxi to ENSO Events over the Past 56 Years. *J. Catastrophol.* **2015**, *30*, 85–90.
51. adhi Rahmawan, G. Tendency for climate-variability-driven rise in Sea level detected in the Altimeter Era in The Marine Waters of Aceh, Indonesia. *Int. J. Remote Sens. Earth Sci. (IJReSES)* **2020**, *16*, 165–178. [CrossRef]
52. Tan, L.; Cai, Y.; An, Z.; Cheng, H.; Shen, C.-C.; Gao, Y.; Edwards, R.L. Decreasing Monsoon Precipitation in Southwest China During the Last 240 Years Associated with the Warming of Tropical Ocean. *Clim. Dyn.* **2017**, *48*, 1769–1778. [CrossRef]
53. Endo, H.; Kitoh, A.; Mizuta, R.; Ose, T. Different Future Changes Between Early and Late Summer Monsoon Precipitation in East Asia. *J. Meteorol. Soc. Japan. Ser. II* **2021**, *99*, 1501–1524. [CrossRef]
54. Gu, W.; Wang, L.; Chen, L. The contrasting interannual variation and mechanism of the first rainy season precipitation before and after the South China Sea summer monsoon onset. *Atmos. Res.* **2024**, *306*, 107455. [CrossRef]
55. Gao, T.; Cao, F.; Dan, L.; Li, M.; Gong, X.; Zhan, J. The Precipitation Variability of the Wet and Dry Season at the Interannual and Interdecadal Scales Over Eastern China (1901–2016): The Impacts of the Pacific Ocean. *Hydrol. Earth Syst. Sci.* **2021**, *25*, 1467–1481. [CrossRef]

56. Pan, X.; Wang, W.; Shao, Q.; Zhang, Y.; Liu, H.; Chen, R. Compound Drought and Heat Waves Variation and Association with SST Modes Across China. *Sci. Total Environ.* **2024**, *907*, 167934. [CrossRef]
57. Wu, J.; Fan, H.; Lin, S.; Zhong, W.; He, S.; Keenlyside, N.; Yang, S. Boosting effect of strong western pole of the Indian Ocean Dipole on the decay of El Niño events. *Npj Clim. Atmos. Sci.* **2024**, *7*, 6. [CrossRef]
58. Debnath, S.; Sinha, M. Rotated empirical orthogonal function analysis for spatio-temporal data analysis. *J. Mech. Contin. Math. Sci.* **2022**, *17*, 21–31. [CrossRef]
59. Shi, P.; Sun, S.; Wang, M.; Li, N.; Wang, J.A.; Jin, Y.; Gu, X.; Yin, W. Climate Change Zoning in China (1961–2010). *Sci. China Earth Sci.* **2014**, *44*, 2294–2306.